ORIGINAL RESEARCH

Green Synthesis of MOF-Mediated pH-Sensitive Nanomaterial AgNPs@ZIF-8 and Its Application in Improving the Antibacterial Performance of AgNPs

Zhiqiang He[1], Huan Yang[1], Yufan Gu [ID][1], Yuhan Xie[1], Jianan Wu[1], Chen Wu[1], Jiawei Song[1], Maofang Zhao[2,3], Da Zong[1], Wenlong Du [ID][1], Jiaju Qiao[1], Yipeng Pang[1–3], Yi Liu [ID][1–3]

[1]Department of Biophysics, School of Life Sciences, Xuzhou Medical University, Xuzhou, Jiangsu, 221004, People's Republic of China; [2]School of Pharmacy, Xuzhou Medical University, Xuzhou, Jiangsu, 221004, People's Republic of China; [3]Jiangsu Key Laboratory of New Drug Research and Clinical Pharmacy, Xuzhou Medical University, Xuzhou, Jiangsu, 221004, People's Republic of China

Correspondence: Yi Liu; Yipeng Pang, Department of Biophysics, School of Life Sciences, Xuzhou Medical University, Xuzhou, Jiangsu, 221004, People's Republic of China, Tel/Fax +86-0516-83262084, Email cbpeliuyinew@163.com; pangyipeng.xzmu@foxmail.com

Purpose: Herein, an emerging drug delivery system was constructed based on zeolite imidazole backbone (ZIF-8) to improve antibacterial defects of nanosilver (AgNPs), such as easily precipitated and highly cytotoxic.

Methods: The homogeneous dispersion of AgNPs on ZIF-8 was confirmed by UV-Vis spectroscopy, FTIR spectroscopy, particle size analysis, zeta potential analysis, and SEM. The appropriate AgNPs loading ratio on ZIF-8 was screened through the cell and antibacterial experiments based on biosafety and antibacterial performance. The optimal environment for AgNPs@ZIF-8 to exert antibacterial performance was probed in the context of bacterial communities under different acid-base conditions. The potential mechanism of AgNPs@ZIF-8 to inhibit the common clinical strains was investigated by observing the biofilm metabolic activity and the level of reactive oxygen species (ROS) in bacteria.

Results: The successful piggybacking of AgNPs by ZIF-8 was confirmed using UV-Vis spectroscopy, FTIR spectroscopy, particle size analysis, zeta potential analysis, and SEM characterization methods. Based on the bacterial growth curve (0–24 hours), the antibacterial ability of AgNPs@ZIF-8 was found to be superior to AgNPs. When the mass ratio of ZIF-8 and AgNPs was 1:0.25, the selection of AgNPs@ZIF-8 was based on its superior antimicrobial efficacy and enhanced biocompatibility. Notably, under weakly acidic bacterial microenvironments (pH=6.4), AgNPs@ZIF-8 demonstrated a more satisfactory antibacterial effect. In addition, experiments on biofilms showed that concentrations of AgNPs@ZIF-8 exceeding 1×MIC resulted in more than 50% biofilm removal. The nanomedicine was found to increase ROS levels upon detecting the ROS concentration in bacteria.

Conclusion: Novel nanocomposites consisting of low cytotoxicity drug carrier ZIF-8 loaded with AgNPs exhibited enhanced antimicrobial effects compared to AgNPs alone. The pH-responsive nano drug delivery system, AgNPs@ZIF-8, exhibited superior antimicrobial activity in a mildly acidic environment. Moreover, AgNPs@ZIF-8 effectively eradicated pathogenic bacterial biofilms and elevated the intracellular level of ROS.

Keywords: MOF, ZIF-8, AgNPs, nanocomplex, ROS, pathogenic biofilm

Introduction

The discovery and use of antibiotics have made a transformative contribution to human health, enabling the effective suppression of pathogenic bacteria.[1] However, the abuse of antibiotics has led to increased resistance to pathogenic microorganisms, especially broad-spectrum antibiotics.[2] Many studies have shown that bacterial resistance leads to hundreds of thousands of deaths each year, so there is an urgent need to find new drugs to replace antibiotics.[3–5] In recent decades, along with the advancement of nanotechnology, monometallic materials have been widely utilized for their

Graphical Abstract
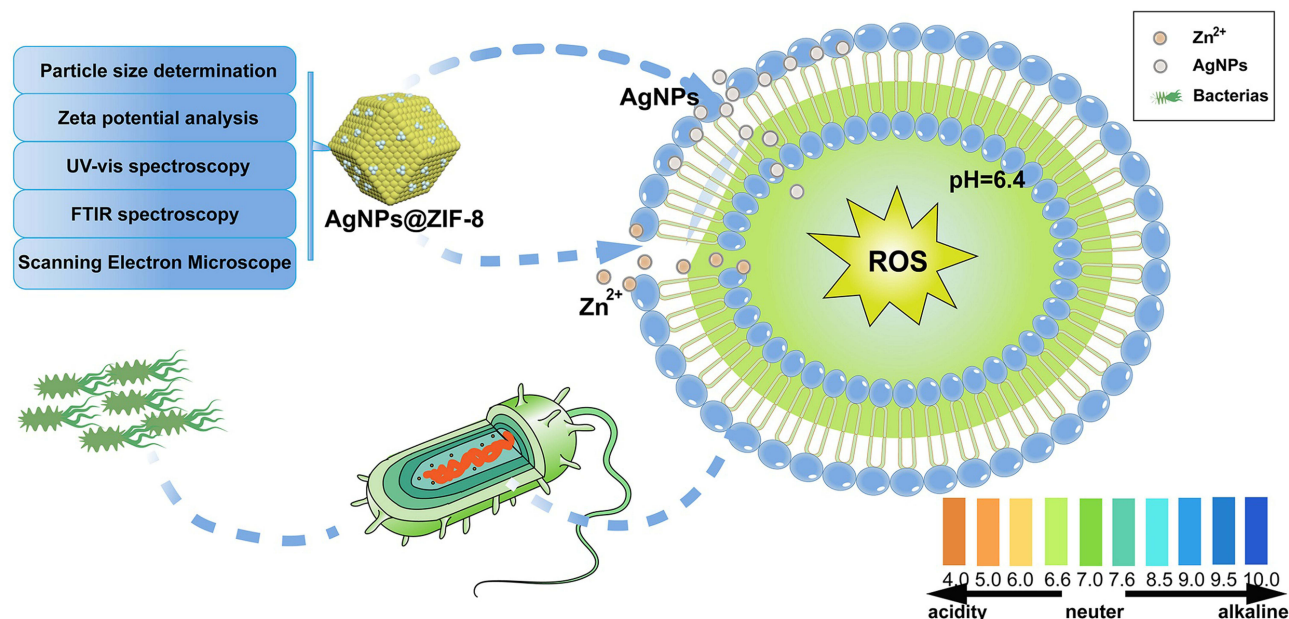
excellent antimicrobial efficacy and environmental friendliness, which can play a part in reducing the use of antibiotics, especially broad-spectrum antibiotics.[6,7] Therefore, developing a new efficient and broad-spectrum inorganic antimicrobial agent is an urgent task.

AgNPs are outstanding in medical devices and wastewater treatment because of their broad-spectrum antibacterial effect, high stability, and vigorous surface activity.[8–10] Our previous studies have confirmed that the green synthesized AgNPs have excellent antibacterial properties.[11] Meanwhile, AgNPs can enter bacteria and release Ag^+ in the presence of protons (H^+) or be oxidized to AgO in the presence of O_2, which can easily bind to negatively charged molecules in bacteria interfere with the normal physiological processes of microorganisms.[12,13] Furthermore, AgNPs possess the ability to engage with the cellular membrane of bacteria, thereby generating superoxide radicals and other reactive oxygen radicals. These radicals have the potential to impair the integrity of bacterial membranes, resulting in leakage of bacterial contents, modification of membrane potential and permeability, and disruption of bacterial ion transport systems. Ultimately, these detrimental effects culminate in the demise of bacteria.[14,15] However, excessive release of metal ions from AgNPs into bacteria and normal tissues may cause respiratory and mild liver damage when deposited in the respiratory and digestive systems.[16–18] Hence, it is essential to investigate how to utilize nanomaterials efficiently.

Presently, Metal Organic Framework(MOF) materials represent a category of crystalline porous nanomaterials characterized by adjustable pore size, resulting from the self-assembly of organic ligands around metal centers. The inherent merits of superior biodegradability, favorable dispersibility, and minimal toxicity render MOFs a highly auspicious nanomaterial.[19,20] Zeolitic imidazolate framework-8 (ZIF-8) is a better pH-responsive drug delivery vehicle with chemical stability in MOFs. In addition, it possesses antibacterial properties because Zn^{2+} can be internalized in bacteria to fracture bacterial cell membranes.[21] ZIF-8 has been effectively applied to mount a variety of nanomaterials to produce sound biological effects. However, it is worth investigating whether AgNPs can be loaded on ZIF-8, mainly to generate pH-sensitive properties of AgNPs@ZIF-8 to produce specific antimicrobial effects.

In the current study, a novel drug delivery platform is developed wherein a pH-sensitive metal carrier ZIF-8 is utilized to piggyback AgNPs, thereby addressing the limitations of AgNPs as nano antimicrobial agents for the inhibition of pathogenic bacteria. The objective of this research is to offer fresh approaches and concepts for the development of non-antibiotic drugs and the rational utilization of MOFs in the design of materials possessing enhanced antimicrobial properties.[22,23]

Materials and Methods

Reagents

Escherichia coli (E. coli), Staphylococcus aureus (S. aureus) and *Acinetobacter baumannii (A. baumannii)* were purchased from Shanghai Luwei Technology Co., Ltd (China). $AgNO_3$ (99.8%) was procured from Sinopharm Chemical Reagent Co., Ltd (China). 2-MIM, $Zn(CH_3COO)_2$, Luria-Bertani and Mueller-Hinton Broth were procured from Shanghai Macklin Bio-technology Co., Ltd (China). Mugwort extract was obtained from Xian Runxue Bio-technology Co., Ltd (China). PBS was acquired by Jiangsu Keygen Biotech Corp.,Ltd. The HT22 cells were procured from Shanghai Gaining Biological Co.

Preparation and Characterization of Materials

Preparation of ZIF-8

0.925 g of $Zn(CH_3COO)_2$ and 4.15 g of 2-MIM were solubilized in 100 mL of methanol. The 2-MIM solution was slowly dropped into the $Zn(CH_3COO)_2$ solution and stirred (1000 rpm, 30 min), followed by sonication (40 kHz, 5 min) and centrifugation (8000 rpm, 15 min). The resulting precipitate was washed 3 times with methanol and desiccated under vacuum for 24 h. The final product, ZIF-8, was preserved at normal temperature, dried, and protected from light.[24]

Synthesis of AgNPs@ZIF-8

20 mg of mugwort extract and 17 mg of $AgNO_3$ were dissolved in 10 mL of ZIF-8, stirred for 20 min and then left in a boiling water bath at 100 °C for 1 h. The solution was filtrated through a 0.22 μm microporous membrane. The $AgNPs_{0.20}$@ZIF-8 solution was prepared by weighing two samples according to the mass ratio of Ag to ZIF-8 of 0.20:1, and the procedure was the same as above.

Characterization of Nanomaterials

Particle Size Determination and Zeta Potential Analysis

Appropriate amounts of sample solutions were prepared for particle size measurement and ZETA potential analysis using a nanoparticle size potentiostat (NICOMP 380NLS).[25]

UV–Vis Spectroscopy

An adequate amount of the sample solution was taken in the cuvette, the blank was corrected with distilled water, and a UV spectrophotometer in 300~800 nm measured its UV absorption spectrum.[26]

FTIR Spectroscopy

The sample solution was made into a powder by rotary evaporation at 60°C and dried in a vacuum oven at 50°C for two hours. The resulting sample powder was added to an infrared spectrometer to observe the characteristic peaks.[27,28]

Scanning Electron Microscope

AgNPs and AgNPs@ZIF-8 were added to the sample tray, and the sample chamber was pumped to vacuum (5×10^{-3} Pa). The voltage was then set to 20 kV for scanning and the brightness and contrast were adjusted. After auto-focusing the sample, adjust the magnification and sharpness to find the homogeneous nanomaterials.[29]

Biocompatibility of Nanomaterials

Cytotoxicity Detection

HT22 cells were distributed in 96-well plates at approximately 4×10^4 cells/mL at a density of 100 μL per well and placed in a cell culture incubator (37°C with a CO_2 level of 5%). HT22 cells were incubated with AgNPs@ZIF-8 at different AgNPs piggyback amounts (20%, 25%, 30%, 35%, 40%) and different concentrations (0 μg/mL, 1 μg/mL, 2.5 μg/mL, 10 μg/mL, 20 μg/mL, 40 μg/mL, 80 μg/mL, 100 μg/mL) given after cell apposition. At the end of the bacterial incubation, the medium containing AgNPs@ZIF-8 was aspirated and washed 3 times with PBS.100 μL of incomplete medium containing 10 μL of CCK-8 assay solution was added and incubated for 1–2 h in an incubator protected from

light. The data were measured at an OD value of 450 nm. The absorbance of the experimental group is expressed as Aa. The absorbance of the control group and the blank group were expressed as Ac and Ab, respectively.[30,31]

$$\text{Ratio of cell survival} = (Aa - Ab)/(Ac - Ab)*100\%$$

In vitro Antimicrobial Activity of the Nanomaterials AgNPs@ZIF-8

Culture of Bacteria

The slant strains were scribed on LB agar plates using the plate scribing isolation method to obtain single colonies, frozen in storage tubes, stored at −20°C and kept away from light. When using the bacterial solution, the concentration of bacterial solution needs to be diluted to 10^8 CFU/mL (The bacteria were measured between 0.4 and 0.5 at the enzyme marker OD_{600}).

Bacterial Growth Curves Test

Different drugs (ZIF-8, AgNPs, AgNPs@ZIF-8) were added to 96-well plates at their different final concentrations (1 μg/mL, 2 μg/mL). 200 μL of MHB and 200 μL of diluted bacterial solution were added to the plates. A blank control and six sets of parallel controls were set up.

The moment of addition of the bacterial solution was noted as 0 h, and its OD value was measured every subsequent hour at 600 nm on an enzyme meter.

Minimum Inhibitory Concentration (MIC) Test

Several sterile centrifuge tubes were prepared to obtain concentrations of 256 μg/mL, 128 μg/mL, 64 μg/mL, 32 μg/mL, 16 μg/mL, 8 μg/mL, 4 μg/mL, 2 μg/mL of a drug (diluted by MHB) according to the multiplicative dilution method, and a centrifuge tube containing only 1 mL of MHB was prepared. 50 μL bacterial solution at a concentration of $1×10^6$ CFU/mL was put in the centrifuge tubes. The results were observed after incubation in a constant temperature incubator at 37°C for 24 h. The procedures for different drug levels ($AgNPs_{0.25}@ZIF-8$, $AgNPs_{0.30}@ZIF-8$, $AgNPs_{0.35}@ZIF-8$, $AgNPs_{0.40}@ZIF-8$) were performed as above. The concentration of the group of drugs that went from turbid to visibly clear was the MIC of the drug.[32]

Minimum Bactericidal Concentration (MBC) Test

The bacterial solution treated by the MIC experiment (MIC, 2 x MIC, 4 x MIC, 8 x MIC) was evenly spread into the solid medium, incubated at 37°C for 24 hours, and the results were recorded. The MBC is defined as the minimum drug concentration at which the colony counts on the plate is less than 5.[33]

In vivo Antimicrobial Activity of the Nanomaterials AgNPs@ZIF-8

Survival Curve of the *Galleria mellonella*

60 larvae of the greater wax borer were taken and divided into 4 groups. They were saline group, drug treatment group, bacterial solution treatment group, and mixed bacterial solution and drug treatment group. Different solutions (20 μL) were injected into the right lower second foot of the larvae with a micro syringe. The number of deaths in each group was recorded every 24 h, and the mortality rate was counted.[34]

Mechanistic Research of Nanomaterials

Bacterial Growth Curve Under pH Conditions

AgNPs@ZIF-8 was added to a 96-well plate at a final concentration of 1 μg/mL. 200 μL of MHB and 200 μL of diluted bacterial solution were added to the 96-well plate. The pH was also adjusted by HCl and NaOH (6.4, 7.4, 8.4), and a blank control and six sets of parallel controls were set up.The moment of adding the bacterial solution was recorded as 0 h, and then its OD value was measured at 600 nm every hour at the wavelength of the enzyme marker.

Biofilm Clearance Test

A bacterial suspension of 0.5 McGill turbidity (concentration of approximately $1×10^8$ CFU/mL) was prepared and diluted 100-fold with MHB. 100 μL of bacterial solution was added to a 96-well plate and incubated at 37°C for 1 hour, allowing biofilm to form in the plate; the bacterial solution was aspirated and washed 3 times with PBS. AgNPs@ZIF-8 were diluted

with sterile water from 4 x MIC multiplication to 1/8 x MIC, 100 μL of each concentration of drug was added to a polystyrene 96-well plate and incubated at 37°C for 1 day. The sterile water group served as a blank control. The solution was aspirated, washed 3 times with PBS and fixed with 100 μL methanol for 15 minutes. Subsequently, the plates were stained with crystalline violet for 10 minutes. The biofilm was dissolved with 100 μL of 95% ethanol and the OD was measured at 620 nm. The minimum drug concentration less than half the OD of the blank control was the BEC50 of AgNPs@ZIF-8 acting on bacteria.[35]

Reactive Oxygen Species Test

Prepare two 2 mL samples of MHB (experimental and control groups) by adding 0.5 mL of AgNPs@ZIF-8 at a concentration of 1/4 MIC to the experimental group. Subsequently, add 1 mL of the bacterial solution to both groups. The prepared system was incubated at 30°C for 6 h, protected from light. After incubation, the supernatant was removed by centrifugation at 3000 rpm and washed three times with PBS. The obtained bacterial cells were mixed with MHB, and DCFH-DA (final concentration of 40 μg/mL) was added. The cells were incubated for half an hour against light and washed three times with PBS. Intracellular ROS levels were observed by fluorescence microscopy.[36–38]

Data Analysis

Data were expressed as mean ± standard deviation (Mean ± SD); two-tailed unpaired Student's *t*-test was used for comparison between two groups; LSD method or SNK-q test was used for variance chi-square. In the diagram shown in this study, "ns" represents no significant difference, "*" represents $p < 0.05$, "**" represents $p < 0.01$, "***" represents $p < 0.001$, and "****" represents $p < 0.0001$.

Results

Synthesis and Characterization of Materials

AgNPs, ZIF-8 and AgNPs@ZIF-8 Characterization

The synthesis of nanocomplex AgNPs@ZIF-8 was shown in Figure 1A.

The SEM analysis results showed that a regular dodecahedral shape of ZIF-8 was successfully synthesized, and the nanosilver particles were dispersed on the surface of the ZIF-8 (Figure 1B and C).

As shown in Figure 1D, FTIR spectra of the synthesized ZIF-8 and AgNPs@ZIF-8 were performed to observe the functional groups of the compounds. The functional groups were separated according to their peaks. In the IR absorption of ZIF-8, the peaks at 3132 cm^{-1}, 2931cm^{-1} were due to the C-H stretching vibration of imidazole. The peaks at 1420cm^{-1} and 1580 cm^{-1} were belonged to the C=N and C-N bonds of imidazole ring. In the IR absorption peaks of AgNPs@ZIF-8, The enhanced absorption peak at 3376 cm^{-1} implied that AgNPs might be piggybacked on ZIF-8. The peak at 767 cm^{-1} indicated the interaction of Ag$^+$ with the imidazole ring.

In Figure 1E, the only peak of ZIF-8 was about 285 nm, the peak of AgNPs was about 433 nm, and the two peaks of AgNPs@ZIF-8 were about 285 nm and 432 nm, respectively. 285 nm were attributed to the Zn present in ZIF-8, and the redshift in the process of nanocomplex assembly was due to the change in the spatial structure and the polarity of the nanocomplex during this process. 433 nm was attributed to AgNPs. Figure 1F showed that the particle sizes of AgNPs, ZIF-8, and AgNPs@ZIF-8 were approximately 89.8 nm, 335.3 nm, and 236.1 nm, respectively. In Figure 1G, the zeta potentials of AgNPs, ZIF-8, and AgNPs @ZIF-8 were 1.39 mv, 0.79 mv, and 2.69 mv, respectively.

Combined with the above experiments, it is confirmed that ZIF-8 successfully hitched on AgNPs, forming a novel AgNPs@ZIF-8 nanocomplex.

Research on the Antibacterial Ability of Nanomaterials

Bacterial Growth Curves Test

The antibacterial ability of nanomaterials is inversely proportional to the bacterial growth activity (0–24 h). Therefore, this approach was applied to measure the antibacterial ability of AgNPs, ZIF-8, and AgNPs@ZIF-8. Figure 2 demonstrated that ZIF-8 exhibited no significant antibacterial ability at low concentrations (1 μg/mL and 2 μg/mL) compared to the control. Meanwhile, bacteria treated with AgNPs were inhibited to some extent. However, as expected, the inhibition of bacterial growth activity by
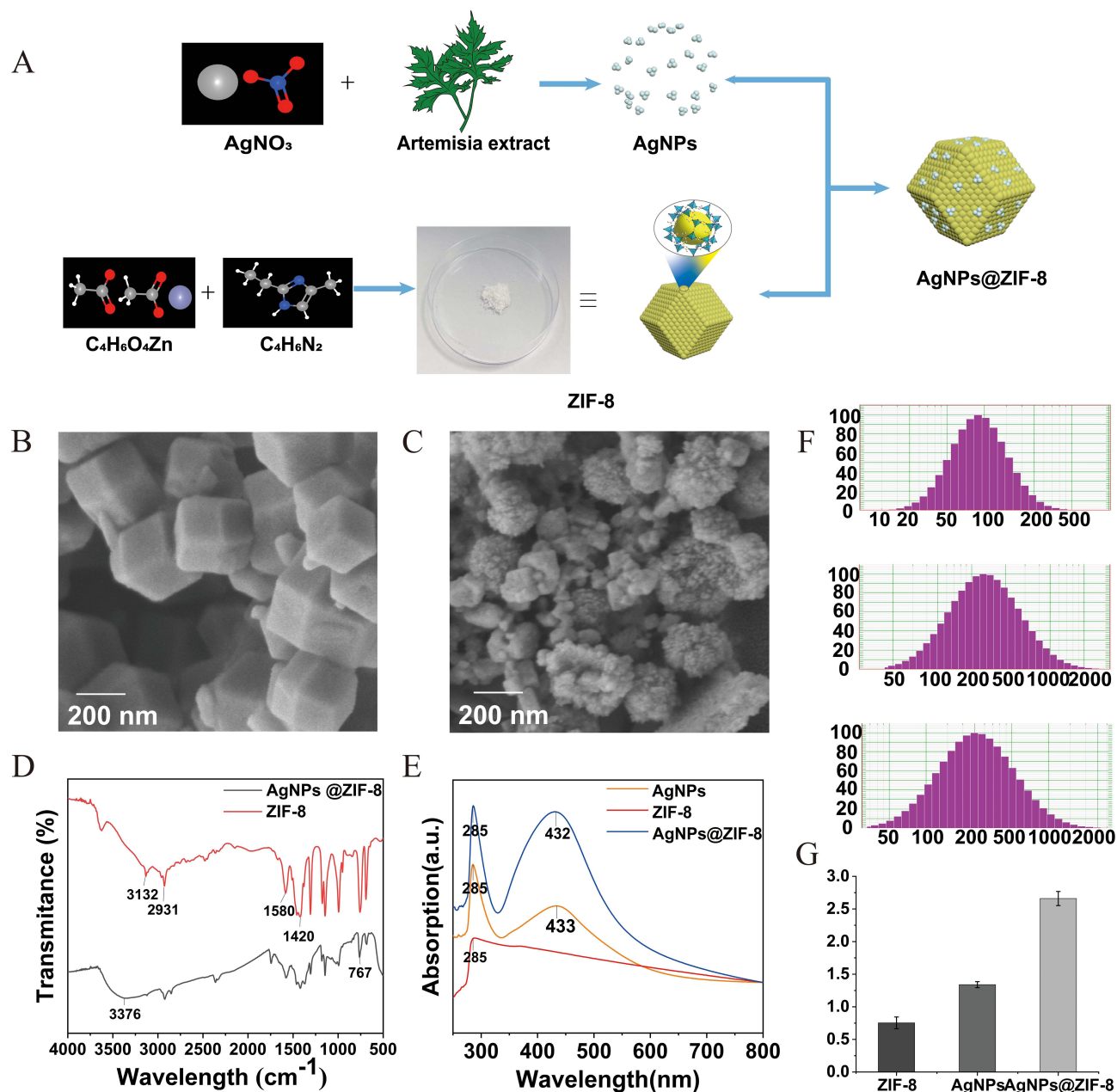
**Figure 1** The characterization of AgNPs, ZIF-8 and AgNPs@ZIF-8.
Notes: (**A**) The synthesis of nanocomplex AgNPs@ZIF-8. (**B** and **C**) Scanning electron microscopy analysis of ZIF-8 and AgNPs@ZIF-8 respectively, Scale bar = 200 nm. (**D**) FT-IR spectroscopy of ZIF-8 and AgNPs@ZIF-8. (**E**) UV-vis spectroscopy of AgNPs, ZIF-8 and AgNPs@ZIF-8, wavelength range is 250–800 nm (**F**) Particle size analysis of AgNPs, ZIF-8 and AgNPs@ZIF-8 and (**G**) Zeta potential analysis of AgNPs, ZIF-8 and AgNPs@ZIF-8, data were expressed as Mean ± SD.

AgNPs@ZIF-8 was significantly more pronounced than the two drugs mentioned above. These results indicated that the inhibition of Gram-negative and Gram-positive bacteria by AgNPs@ZIF-8 was significantly better than the same concentration of ZIF-8 and AgNPs.

Selection of Nanomaterials with the Best Loading Ratio

Minimum Inhibitory Concentration Test

As presented in Figure 3, the MIC of $AgNPs_{0.20}@ZIF-8$ for the three bacteria studied was 32 μg/mL, the MIC of $AgNPs_{0.25}@ZIF-8$, $AgNPs_{0.30}@ZIF-8$, and $AgNPs_{0.35}@ZIF-8$ for the three bacteria studied was 16 μg /mL. In comparison, the MIC of $AgNPs_{0.40}@ZIF-8$ was 8 μg/mL for the three investigated bacteria.
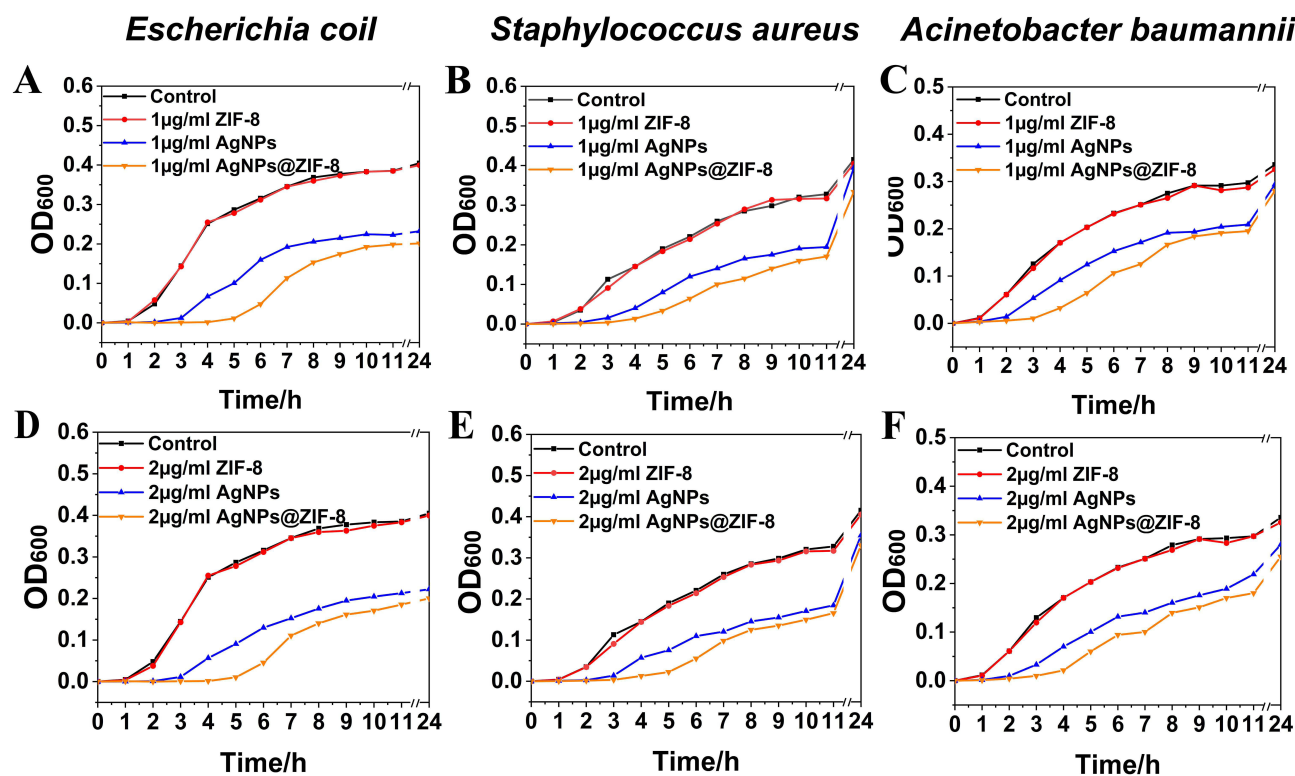
Figure 2 The results of the bacterial growth curves of the control group and the 1 μg/mL AgNPs@ZIF-8 and 2 μg/mL AgNPs@ZIF-8.
Notes: (**A** and **D**) AgNPs@ZIF-8 against *Escherichia coli*, (**B** and **E**) AgNPs@ZIF-8 against *Staphylococcus aureus*, (**C** and **F**) AgNPs@ZIF-8 against *Acinetobacter baumannii*.

Minimum Bactericidal Concentration Test

MBC experiments were employed to further investigate the antibacterial performance of AgNPs@ZIF-8 synthesized from AgNPs and ZIF-8 at different mass ratios. As illustrated in Figure 4, the MBCs of AgNPs$_{0.20}$@ZIF-8 were 128 μg/mL, 64 μg/mL, and 128 μg/mL for *E. coli, S. aureus* and *A. baumannii*, respectively. AgNPs$_{0.25}$@ZIF-8, AgNPs$_{0.30}$@ZIF-8, AgNPs$_{0.35}$@ZIF-8 was discovered to be more effective against *E. coli, S. aureus*, and *A. baumannii* were 64 μg/mL, 32 μg/mL and 64 μg/mL, respectively, and AgNPs$_{0.4}$@ZIF-8 were 16 μg/mL, 16 μg/mL and 32 μg/mL for *E. coli, S. aureus*, and *A. baumannii*, respectively.

In vivo Antimicrobial Activity of the Nanomaterials AgNPs@ZIF-8

Larvae of the *Galleria mellonella* Experiment

As shown in the Figure 5, at the 7 day, no larvae died in the saline treatment group, 2 in the drug treatment group, 13 in the bacterial solution treatment group, and 9 in the mixed bacterial solution and drug treatment group. After log-rank analysis, the results showed that there was no significant difference between the saline treated group and the drug treated group, and the mortality of infected larvae after drug treatment was significantly reduced.

Biocompatibility of Nanomaterials

Cytotoxicity Detection Test

The biocompatibility of AgNPs@ZIF-8 synthesized from different mass ratios of AgNPs and ZIF-8 was verified via Cell Counting Kit-8 (CCK-8) experiments. As shown in Figure 6, the cellular activities of AgNPs$_{0.20}$@ZIF-8, AgNPs$_{0.25}$@ZIF-8, AgNPs$_{0.30}$@ZIF-8, AgNPs$_{0.35}$@ZIF-8, and AgNPs$_{0.40}$@ZIF-8 were found to be about 82%, 72%, 62%, 57% and 51% at 5 μg/mL concentrations, respectively; 10 μg/mL concentrations were approximately 73%, 61%, 43%, 39%, and 28%.

Based on the biocompatibility and antibacterial ability of the nanomaterials, AgNPs$_{0.25}$@ZIF-8 showed a better overall ability by MIC, MBC, and CCK-8 experiments.
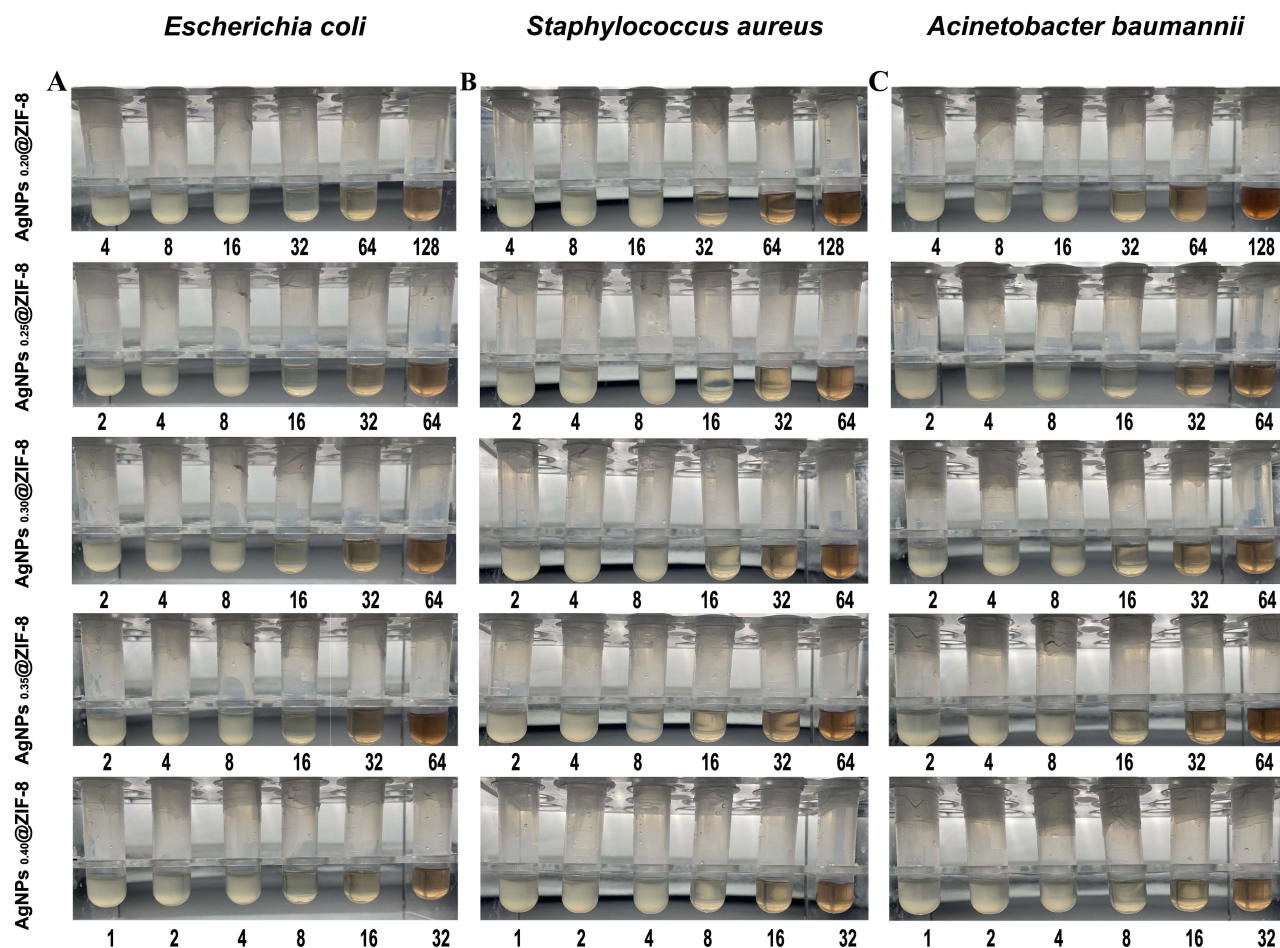
Figure 3 The MIC (μg/mL) test results of the control group and different concentrations of AgNPs@ZIF-8* groups on (**A**) *Escherichia coli*, (**B**) *Staphylococcus aureus* and (**C**) *Acinetobacter baumannii*.

Notes: AgNPs@ZIF-8* indicates AgNPs$_{0.20}$@ZIF-8, AgNPs$_{0.25}$@ZIF-8, AgNPs$_{0.30}$@ZIF-8, AgNPs$_{0.35}$@ZIF-8 and AgNPs$_{0.40}$@ZIF-8. The concentration of the group of drugs that went from turbid to visibly clear was the MIC of the drug.

Investigation of the Optimal Environment for Nanomaterials to Exert Antibacterial Effects

Bacterial Growth Curve Under pH Conditions

The pH of the MHB was altered to mimic the weakly acidic environment caused by a significant infection of pathogenic microorganisms. As shown in Figure 7, there was no significant difference in the ability of AgNPs@ZIF-8 to inhibit pathogenic microorganisms in alkaline (pH=8.4) and neutral (pH=7.4) environments. In comparison, the inhibitory effect of AgNPs@ZIF-8 on bacterial growth activity was more pronounced in an acidic (pH=6.4) environment.

Study on the Mechanism of Antibacterial Effect of Materials

Reactive Oxygen Species Test

As shown in Figure 8A, bacterial cells labeled with probe H2DCFH-DA produced brighter fluorescence with higher levels of cellular reactive oxygen species after treatment with 8 μg/mL of AgNPs$_{0.25}$@ZIF-8 relative to the control group. The fluorescence intensity was approximately 0.8 A.U in the control group and 1.6 A.U in the drug-treated group. The quantitative analysis of the fluorescence intensity of the treated and normal groups was shown in Figure 8B.
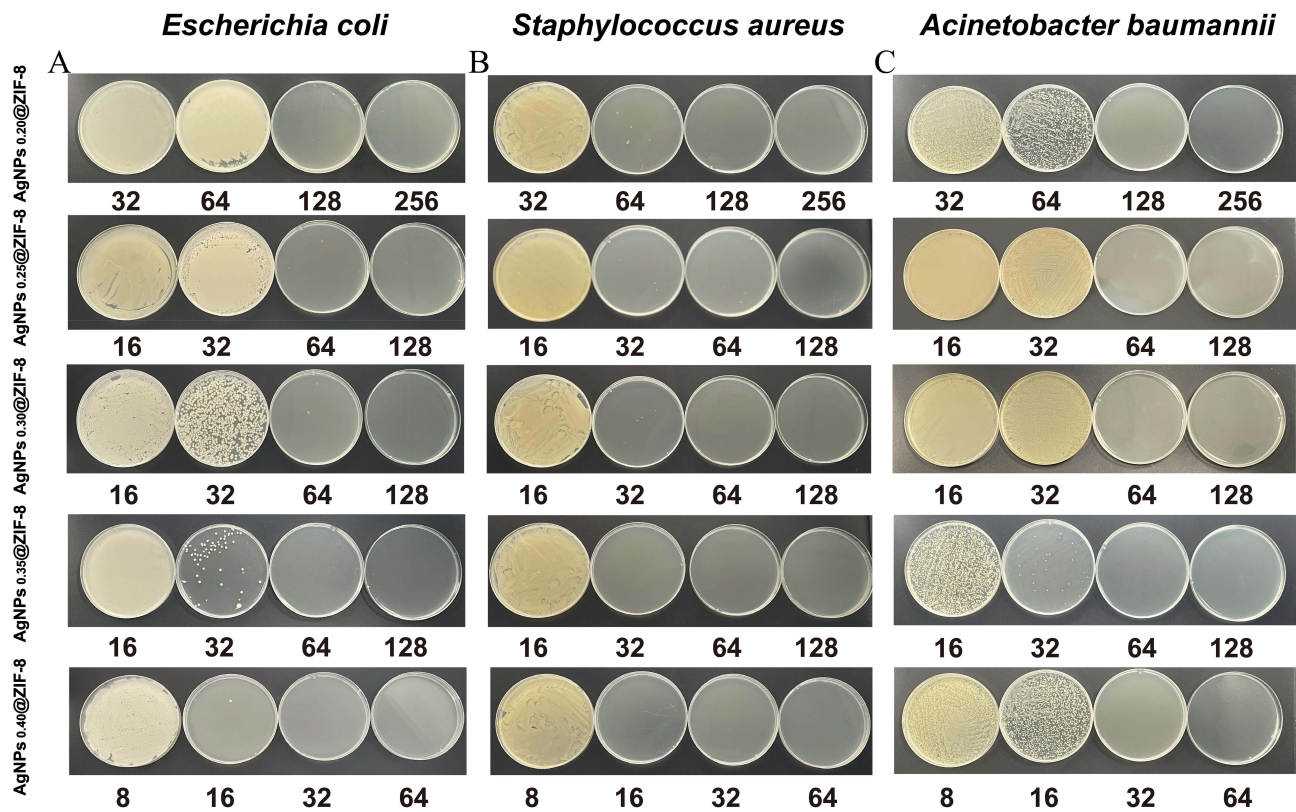
Figure 4 The MBC (μg/mL) test results of the control group and the different concentrations of AgNPs@ZIF-8* group on (**A**) *Escherichia coli*, (**B**) *Staphylococcus aureus*, (**C**) *Acinetobacter baumannii*.
Notes: AgNPs@ZIF-8* indicates AgNPs$_{0.20}$@ZIF-8, AgNPs$_{0.25}$@ZIF-8, AgNPs$_{0.30}$@ZIF-8, AgNPs$_{0.35}$@ZIF-8 and AgNPs$_{0.40}$@ZIF-8. The MBC is defined as the minimum drug concentration at which the colony count on the plate is less than 5.
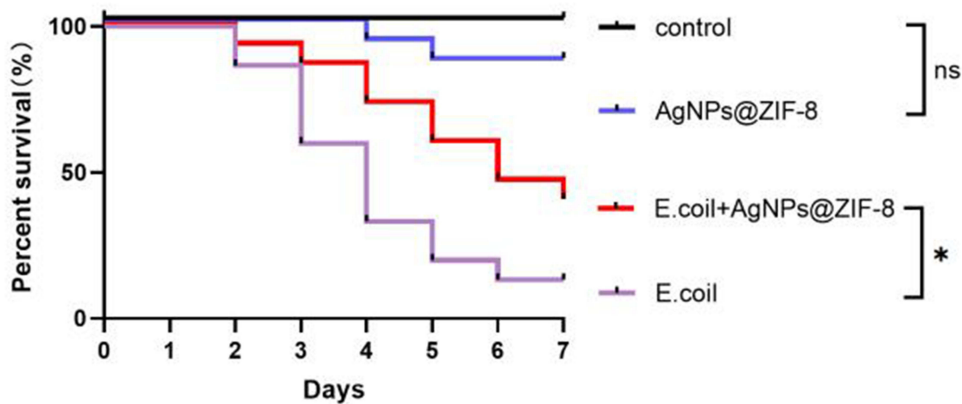

Figure 5 In vivo effects of AgNPs@ZIF-8 on *E. coli* activity.
Notes: Survival curve of *Galleria mellonella* larvae. *$p < 0.05$; ns, $p > 0.05$ according to log rank analysis. Dead larvae have black body color, surviving larvae have no body color change.

Pathogenic Biofilm Eradication Concentration Test

As shown in Figure 8C, the biofilm metabolic activity of *E. coli* was reduced to less than 50% after treatment with AgNPs@ZIF-8 at 1/2×MIC compared to the control. The BEC50 of AgNPs@ZIF-8 against *E. coli* was 1/2×MIC. The BEC50 of AgNPs@ZIF-8 against *S. aureus* and *A. baumannii* were both 1× MIC.
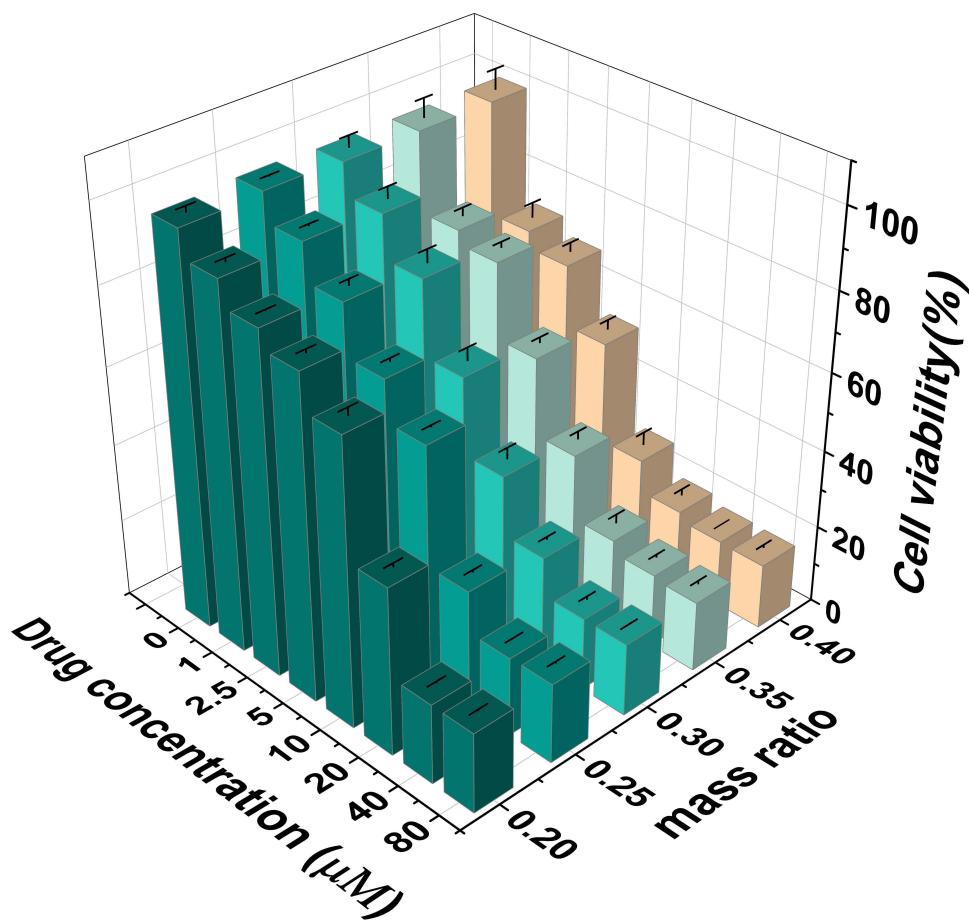
Figure 6 Effects of AgNPs@ZIF-8 on the viability of HT-22 cells.
Note: Cell viability was determined by MTT assay after treating cells with a series of concentrations of AgNPs@ZIF-8* (0, 1, 2.5, 5, 10, 20, 40, 80, 100) for 24 h.
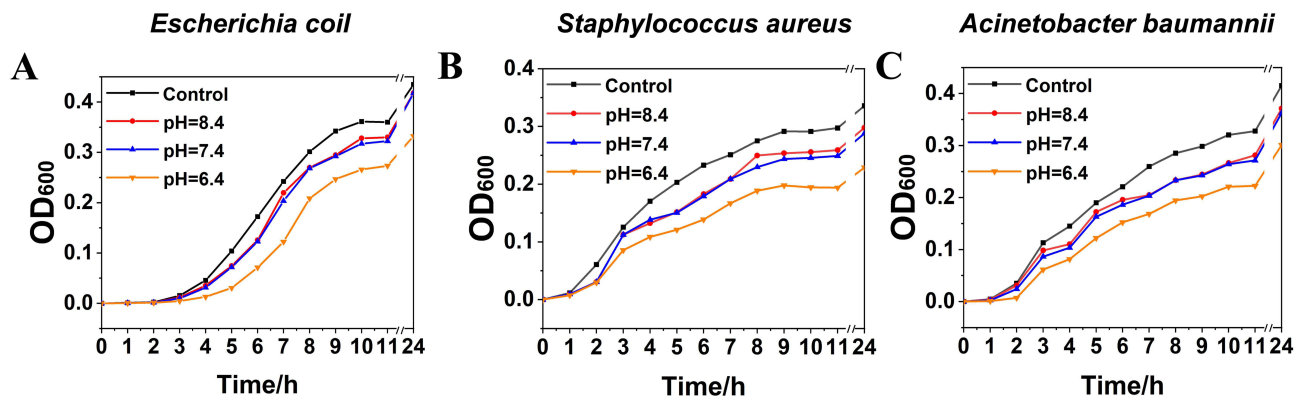

Figure 7 Survival curves of strains.
Notes: (**A**) *Escherichia coli*, (**B**) *Staphylococcus aureus* and (**C**) *Acinetobacter baumannii* under different pH (6.4, 7.4, 8.4) conditions.

Discussions

The complications caused by pathogenic microorganisms have been a challenge for clinical treatment.[39] The misuse of antibiotics has increased the tolerance of pathogenic microorganisms,[40] which is a severe threat to human health and environmental safety. Previous studies by Pawe·Pomastowski et al had noted the importance of nanomaterials for

Figure 8 The mechanism of antibacterial activity of AgNPs@ZIF-8.
Notes: (**A**) Relative ROS level of fluorescence microscope images of *Escherichia coli*. Green fluorescence represents the level of ROS, (**B**) fluorescence intensity of the control group and 8 μg/mL AgNPs@ZIF-8-treated bacteria detected under fluorescence microscope and (**C**) the results of the pathogenic biofilm activity of the control group and different concentrations AgNPs@ZIF-8 group against three strains. Data were analyzed by *t*-test. **$p < 0.01$, ***$p < 0.001$, ****$p < 0.0001$ vs control group.

controlling pathogenic microorganisms, which could effectively inhibit pathogenic microorganisms and were less likely to develop tolerance.[41,42] Therefore, utilizing nanomaterials efficiently has become the focus of current research.

Our previous studies confirmed that AgNPs were excellent inorganic antimicrobial agents with broad-spectrum antibacterial properties.[11] Moreover, AgNPs exhibit a reduced propensity for developing resistance against pathogenic microorganisms. Nevertheless, they encounter challenges such as significant cytotoxicity and a tendency to aggregate. In this study, we aimed to explore the potential of AgNPs@ZIF-8, a nanomaterial formed by attaching AgNPs onto MOF, to enhance the broad-spectrum antibacterial properties of AgNPs. The bacterial growth curves showed that a quantitative (small) amount of AgNPs loaded onto the ZIF-8 performed a better antibacterial effect than the same amount of AgNPs alone. According to the review by Hani Nasser

Abdelhamid, the encapsulated antimicrobial agent ZIF-8 exhibited superior biological activity compared to the free antimicrobial agent.[21] Therefore, we infer that the above experimental results are attributed to the piggyback function of ZIF-8.

It is crucial to determine the appropriate ratio of AgNPs to ZIF-8 to achieve good antimicrobial properties and low cytotoxicity of AgNPs@ZIF-8 for practical applications. We constructed AgNPs@ZIF-8 with ZIF-8 and AgNPs based on previous research literature, in which the mass ratios of ZIF-8 and AgNPs were 1:0.20; 1:0.25; 1:0.30; 1:0.35; 1:0.40, respectively. The MIC of *E. coli, A. baumannii* and *S. aureus* in the $AgNPs_{0.25}@ZIF-8$ group was 16 μg/mL. The MBC of the above three bacteria in $AgNPs_{0.25}@ZIF-8$ was 64 μg/mL, 64 μg/mL and 32 μg/mL, respectively. Metal ions are more likely to cause neurotoxicity,[43] so it was necessary to focus on the effect of this nanomaterial on the survival of HT-22 neuronal cells.Through CCK-8 assay, we found that $AgNPs_{0.25}@ZIF-8$, the cellular activity at MIC concentration was about 60%. Considering the above experiments and practical clinical applications, $AgNPs_{0.25}@ZIF-8$ was chosen as the study subject because of its lower cytotoxicity and better antibacterial effect.[44]

In addition, common clinical pathogens such as *E. coli* and *S. aureus* are parthenogenic anaerobes that produce acid and gas during anaerobic respiration, resulting in a decrease in pH in the colony environment.[45] Therefore, the ability to inhibit bacterial activity in an acidic environment is worth considering when evaluating the antimicrobial effect of nanomaterials. In this paper, the acidic environment due to heavy bacterial contamination was simulated by adjusting the pH of the culture medium MHB. By studying the growth curves of bacteria over 24 h, it was observed that all three bacteria exhibited: the antibacterial ability of AgNPs@ZIF-8 in weakly alkaline conditions (pH=8.4) was similar to the antibacterial ability in neutral conditions (pH=7.4); while in weakly acidic conditions (pH=6.4), the bacteria were more significantly inhibited by AgNPs@ZIF-8. We inferred that the weakly acidic conditions are more favorable for the AgNPs@ZIF-8 to exert its antibacterial ability. There are two main reasons to explain this phenomenon. Firstly, among the components of ZIF-8: zinc is the second most biologically abundant transition metal, and the imidazole group is an essential component of the amino acid histidine. The coordination between zinc and imidazole ions dissociates when weak acids are present, which makes the drug release pH-responsive.[46] In addition, we propose the conjecture that ZIF-8 releases Zn^+, which increases the permeability of the bacterial cell membrane in a weak acid environment. In this case, Ag^+, which plays an efficient antibacterial role, can more easily enter the bacteria and disturb their internal microenvironment to achieve better antibacterial performance. The AgNPs were piggybacked on the ZIF-8 to synthesize a new antibacterial AgNPs@ZIF-8, and its antibacterial effect was verified.

Herein, the potential mechanism of the antibacterial effect of AgNPs@ZIF-8 was investigated, and it was found that the material increased the level of ROS in the bacterial community and effectively removed the biofilm of the bacterial community, which might be the mechanism of the good antibacterial effect of the nanocomposite. It also gave full play to the carrier role of ZIF-8 in a weakly acidic environment, which could reduce the amount of AgNPs. It provides a theoretical basis and new ideas for the prevention and control of infections of a variety of pathogenic bacteria and guides the rational design of high antibacterial performance drugs and avoidance of potential dangers of antibacterial agents.[47–50]

Conclusion

In this study, a novel nanocomposite of AgNPs@ZIF-8 was synthesized, leveraging the beneficial properties of the low cytotoxic drug carrier ZIF-8 and antibacterial AgNPs. It was observed that AgNPs@ZIF-8 displayed superior antimicrobial activity compared to AgNPs alone, with the optimal mass ratio of ZIF-8 and AgNPs determined to be 1:0.25. Additionally, the pH-responsive nature of AgNPs@ZIF-8 was demonstrated, exhibiting enhanced antimicrobial efficacy in a weakly acidic environment. Moreover, our findings demonstrate that AgNPs@ZIF-8 exhibits significant efficacy in eradicating pathogenic bacterial biofilms and inducing elevated levels of ROS within the bacterial cells, thereby impeding their proliferation and viability. Consequently, our results indicate that AgNPs@ZIF-8 holds great potential as a nanomaterial for antimicrobial purposes.

Acknowledgments

Funding

Disclosure

The authors report no conflicts of interest in this work.

References

1. Cook MA, Wright GD. The past, present, and future of antibiotics. *Sci Transl Med*. 2022;14:eabo7793. doi:10.1126/scitranslmed.abo7793
2. Mancuso G, Midiri A, Gerace E, Biondo C. Bacterial antibiotic resistance: the most critical pathogens. *Pathogens*. 2021;10(10):1310. doi:10.3390/pathogens10101310
3. Ibrahim S, Al-Saryi N, Al-Kadmy IMS, Aziz SN. Multidrug-resistant Acinetobacter baumannii as an emerging concern in hospitals. *Mol Biol Rep*. 2021;48:6987–6998. doi:10.1007/s11033-021-06690-6
4. Reynolds D, Burnham JP, Vazquez Guillamet C, et al. The threat of multidrug-resistant/extensively drug-resistant gram-negative respiratory infections: another pandemic. *Eur Respir Rev*. 2022;31:220068. doi:10.1183/16000617.0068-2022
5. Urban-Chmiel R, Marek A, Stępień-Pyśniak D, et al. Antibiotic resistance in bacteria-a review. *Antibiotics*. 2022;11:1079. doi:10.3390/antibiotics11081079
6. Jampilek J. Drug repurposing to overcome microbial resistance. *Drug Discov Today*. 2022;27:2028–2041. doi:10.1016/j.drudis.2022.05.006
7. Varela MF, Stephen J, Lekshmi M, et al. Bacterial resistance to antimicrobial agents. *Antibiotics*. 2021;10:593. doi:10.3390/antibiotics10050593
8. Eleraky NE, Allam A, Hassan SB, Omar MM. nanomedicine fight against antibacterial resistance: an overview of the recent pharmaceutical innovations. *Pharmaceutics*. 2020;12:142. doi:10.3390/pharmaceutics12020142
9. Gad El-Rab SMF, Halawani EM, Alzahrani SSS. Biosynthesis of silver nano-drug using Juniperus excelsa and its synergistic antibacterial activity against multidrug-resistant bacteria for wound dressing applications. *Biotech*. 2021;11:255. doi:10.1007/s13205-021-02782-z
10. Mohammadinejat M, Sepahi AA, Alipour E. Antibacterial and anti-biofilm activities of silver nano particles conjugated to chitosan against multi-drug resistant bacteria. *Clin Lab*. 2023;69. doi:10.7754/Clin.Lab.2022.220315
11. Hu L, Yang X, Yin J, et al. Combination of AgNPs and domiphen is antimicrobial against biofilms of common pathogens. *Int J Nanomedicine*. 2021;16:7181–7194. doi:10.2147/IJN.S334133
12. Chandraker SK, Kumar R. Biogenic biocompatible silver nanoparticles: a promising antibacterial agent. *Biotechnol Genet Eng Rev*. 2022;1–35. doi:10.1080/02648725.2022.2106084
13. Qamer S, Romli MH, Che-Hamzah F, et al. Systematic review on biosynthesis of silver nanoparticles and antibacterial activities: application and theoretical perspectives. *Molecules*. 2021;26:5057. doi:10.3390/molecules26165057
14. Liehai H, Zhu X, Yu S, et al. Research progress of nano-silver antibacterial application. *Chin J Antib*. 2020;45(8):745–750.
15. Xie W, Chen J, Cheng X, et al. Multi-mechanism antibacterial strategies enabled by synergistic activity of metal-organic framework-based nanosystem for infected tissue regeneration. *Small*. 2023;19:e2205941. doi:10.1002/smll.202205941
16. Jiang Y, Huang J, Wu X, Ren Y, Li Z, Ren J. Controlled release of silver ions from AgNPs using a hydrogel based on konjac glucomannan and chitosan for infected wounds. *Int J Biol Macromol*. 2020;149:148–157. doi:10.1016/j.ijbiomac.2020.01.221
17. Hashim M, Mujahid H, Hassan S, et al. Implication of nanoparticles to combat chronic liver and kidney diseases: progress and perspectives. *Biomolecules*. 2022;12:1337. doi:10.3390/biom12101337
18. Shi L, Pan R, Lin G, et al. Lactic acid bacteria alleviate liver damage caused by perfluorooctanoic acid exposure via antioxidant capacity, biosorption capacity and gut microbiota regulation. *Ecotoxicol Environ Saf*. 2021;222:112515. doi:10.1016/j.ecoenv.2021.112515
19. Giliopoulos D, Zamboulis A, Giannakoudakis D, Bikiaris D, Triantafyllidis K. Polymer/Metal Organic Framework (MOF) nanocomposites for biomedical applications. *Molecules*. 2020;25:185. doi:10.3390/molecules25010185
20. Yang J, Yang Y-W. Metal-organic frameworks for biomedical applications. *Small*. 2020;16:e1906846. doi:10.1002/smll.201906846
21. Abdelhamid HN. Zeolitic Imidazolate Frameworks (ZIF-8) for biomedical applications: a review. *Curr Med Chem*. 2021;28:7023–7075. doi:10.2174/0929867328666210608143703
22. Ravinayagam V, Rehman S. Zeolitic imidazolate framework-8 (ZIF-8) doped TiZSM-5 and mesoporous carbon for antibacterial characterization. *Saudi J Biol Sci*. 2020;27(7):1726–1736. doi:10.1016/j.sjbs.2020.05.016
23. Sun M, Liu Y, Jiao K, et al. A periodontal tissue regeneration strategy via biphasic release of zeolitic imidazolate framework-8 and FK506 using a uniaxial electrospun janus nanofiber. *J Mater Chem B*. 2022;10:765–778. doi:10.1039/d1tb02174e
24. Wang Q, Sun Y, Li S, Zhang P, Yao Q. Synthesis and modification of ZIF-8 and its application in drug delivery and tumor therapy. *RSC Adv*. 2020;10:37600–37620. doi:10.1039/d0ra07950b
25. Krishnaswami V, Sugumaran A, Perumal V, et al. Nanoformulations - insights towards characterization techniques. *Curr Drug Targets*. 2022;23 (14):1330–1344. doi:10.2174/1389450123666220822094248
26. Quevedo AC, Guggenheim E, Briffa SM, et al. UV-Vis spectroscopic characterization of nanomaterials in aqueous media. *J Vis Exp*. 2021. doi:10.3791/61764
27. Sankareswaran M, Periakaruppan R, Sasivarnam M, Danaraj J, Dhanasekaran S, Abomughaid MM. Bio-fabrication of bio-inspired silica nanomaterials from bryophyllum pinnatum leaf for agricultural applications. *Appl Biochem Biotechnol*. 2022;194:4266–4277. doi:10.1007/s12010-022-03996-4
28. Kamnev AA, Dyatlova YA, Kenzhegulov OA, et al. Fourier Transform Infrared (FTIR) spectroscopic analyses of microbiological samples and biogenic selenium nanoparticles of microbial origin: sample preparation effects. *Molecules*. 2021;26(4):1146. doi:10.3390/molecules26041146
29. Kim H, Murata MM, Chang H, et al. Optical and electron microscopy for analysis of nanomaterials. *Adv Exp Med Biol*. 2021;1309:277–287. doi:10.1007/978-981-33-6158-4_12
30. Liu L-W, Yang M-Y, Zhou M, Li -J-J, Liu B, Pan -Y-Y. Improvement of cytotoxicity of autologous CIKs from patients with breast cancer to MCF-7 cells by suppressed PD-1 expression. *Cancer Biomark*. 2017;20:609–615. doi:10.3233/CBM-170588

31. Ou P, Hao C, Liu J, et al. Cytocompatibility of Ti-xZr alloys as dental implant materials. *J Mater Sci Mater Med*. 2021;32(5):50. doi:10.1007/s10856-021-06522-w

32. Parvekar P, Palaskar J, Metgud S, Maria R, Dutta S. The Minimum Inhibitory Concentration (MIC) and Minimum Bactericidal Concentration (MBC) of silver nanoparticles against staphylococcus aureus. *Biomater Investig Dent*. 2020;7:105–109. doi:10.1080/26415275.2020.1796674

33. Rodríguez-Melcón C, Alonso-Calleja C, García-Fernández C, Carballo J, Capita R. Minimum Inhibitory Concentration (MIC) and Minimum Bactericidal Concentration (MBC) for twelve antimicrobials (Biocides and Antibiotics) in eight strains of listeria monocytogenes. *Biology*. 2021;11(1):46. doi:10.3390/biology11010046

34. Sun Y, Tan L, Yao Z, Gao L, Yang J, Zeng T. In vitro and in vivo interactions of TOR Inhibitor AZD8055 and azoles against pathogenic fungi. *Microbiol Spectr*. 2022;10:e0200721. doi:10.1128/spectrum.02007-21

35. Zheng Y, Wang D, Ma LZ. Effect of polyhexamethylene biguanide in combination with undecylenamidopropyl Betaine or PslG on biofilm clearance. *Int J Mol Sci*. 2021;22:768. doi:10.3390/ijms22020768

36. Espinoza EM, Røise JJ, Li I-C, Das R, Murthy N. Advances in imaging reactive oxygen species. *J Nucl Med*. 2021;62:457–461. doi:10.2967/jnumed.120.245415

37. Cheung EC, Vousden KH. The Role of ROS in tumour development and progression. *Nat Rev Cancer*. 2022;22:280–297. doi:10.1038/s41568-021-00435-0

38. Yang B, Chen Y, Shi J. Reactive Oxygen Species (ROS)-Based Nanomedicine. *Chem Rev*. 2019;119:4881–4985. doi:10.1021/acs.chemrev.8b00626

39. Gebrayel P, Nicco C, Al Khodor S, et al. Microbiota medicine: towards clinical revolution. *J Transl Med*. 2022;20:111. doi:10.1186/s12967-022-03296-9

40. Qin L, Tao Y. The abuse of antibiotics and the harm to the human body. *Health Vision*. 2013;21:288.

41. Pomastowski P, Król-Górniak A, Railean-Plugaru V, Buszewski B. Zinc oxide nanocomposites-extracellular synthesis, physicochemical characterization and antibacterial potential. *Materials*. 2020;13:4347. doi:10.3390/ma13194347

42. Al-Radadi NS, Hussain T, Hussain T, et al. Novel biosynthesis, characterization and bio-catalytic potential of green algae (Spirogyra hyalina) mediated silver nanomaterials. *Saudi J Biol Sci*. 2022;29(1):411–419. doi:10.1016/j.sjbs.2021.09.013

43. Li Z, Liu Y, Wei R, Yong VW, Xue M. The important role of zinc in neurological diseases. *Biomolecules*. 2022;13:28. doi:10.3390/biom13010028

44. Holliday SL, Beuchat LR. Viability of salmonella, Escherichia coli O157: H7, and listeria monocytogenes in yellow fat spreads as affected by storage temperature. *J Food Prot*. 2003;66:549–558. doi:10.4315/0362-028x-66.4.549

45. Chandhru M, Logesh R, Kutti Rani S, Ahmed N, Vasimalai N. Green synthesis of silver nanoparticles from plant latex and their antibacterial and photocatalytic studies. *Environ Technol*. 2022;43:3064–3074. doi:10.1080/09593330.2021.1914181

46. Khan MI, Shah S, Faisal S, et al. Monotheca buxifolia driven synthesis of zinc oxide nano material its characterization and biomedical applications. *Micromachines*. 2022;13:668. doi:10.3390/mi13050668

47. Faisal S, Ullah R, Alotaibi A, Zafar S, Rizwan M, Tariq MH. Biofabrication of silver nanoparticles employing biomolecules of paraclostridium benzoelyticum strain: its characterization and their in-vitro antibacterial, anti-aging, anti-cancer and other biomedical applications. *Microsc Res Tech*. 2023;86:846–861. doi:10.1002/jemt.24362

48. Faisal S, Khan MA, Jan H, et al. Redaina, null edible mushroom (Flammulina Velutipes) as biosource for silver nanoparticles: from synthesis to diverse biomedical and environmental applications. *Nanotechnology*. 2021;32:065101. doi:10.1088/1361-6528/abc2eb

49. Faisal S, Jan H, Alam I, et al. In vivo analgesic, anti-inflammatory, and anti-diabetic screening of bacopa monnieri-synthesized copper oxide nanoparticles. *ACS Omega*. 2022;7(5):4071–4082. doi:10.1021/acsomega.1c05410

50. Jan H, Shah M, Andleeb A, et al. Plant-Based Synthesis of Zinc Oxide Nanoparticles (ZnO-NPs) using aqueous leaf extract of aquilegia pubiflora: their antiproliferative activity against HepG2 cells inducing reactive oxygen species and other in vitro properties. *Oxid Med Cell Longev*. 2021;2021:4786227. doi:10.1155/2021/4786227